



# Kinetic and Sequence-Structure-Function Analysis of LinB Enzyme Variants with $\beta$ - and $\delta$ -Hexachlorocyclohexane

Rinku Pandey<sup>1,2,3a</sup>, Del Lucent<sup>2,3b</sup>, Kirti Kumari<sup>1,4ab</sup>, Pooja Sharma<sup>1,4ac</sup>, Rup Lal<sup>4</sup>, John G. Oakeshott<sup>1</sup>, Gunjan Pandey<sup>1\*</sup>

**1** CSIRO Ecosystem Sciences, Acton, ACT, Australia, **2** CSIRO Center for Materials Science and Engineering, Parkville VIC, Australia, **3** Division of Engineering and Physics, Wilkes University, Wilkes-Barre, Pennsylvania, United States of America, **4** Department of Zoology, University of Delhi, Delhi, India

## Abstract

Organochlorine insecticide hexachlorocyclohexane (HCH) has recently been classified as a 'Persistent Organic pollutant' by the Stockholm Convention. The LinB haloalkane dehalogenase is a key upstream enzyme in the recently evolved Lin pathway for the catabolism of HCH in bacteria. Here we report a sequence-structure-function analysis of ten naturally occurring and thirteen synthetic mutants of LinB. One of the synthetic mutants was found to have ~80 fold more activity for  $\beta$ - and  $\delta$ -hexachlorocyclohexane. Based on detailed biophysical calculations, molecular dynamics and ensemble docking calculations, we propose that the latter variant is more active because of alterations to the shape of its active site and increased conformational plasticity.

**Citation:** Pandey R, Lucent D, Kumari K, Sharma P, Lal R, et al. (2014) Kinetic and Sequence-Structure-Function Analysis of LinB Enzyme Variants with  $\beta$ - and  $\delta$ -Hexachlorocyclohexane. PLoS ONE 9(7): e103632. doi:10.1371/journal.pone.0103632

**Editor:** Isabelle Andre, University of Toulouse - Laboratoire d'Ingénierie des Systèmes Biologiques et des Procédés, France

**Received:** May 13, 2014; **Accepted:** June 29, 2014; **Published:** July 30, 2014

**Copyright:** © 2014 Pandey et al. This is an open-access article distributed under the terms of the Creative Commons Attribution License, which permits unrestricted use, distribution, and reproduction in any medium, provided the original author and source are credited.

**Data Availability:** The authors confirm that all data underlying the findings are fully available without restriction. All relevant data are within the paper and its Supporting Information files.

**Funding:** Part of the work was supported by the Indian Australian Strategic Research Fund and Commonwealth Scientific and Industrial Research Organisation's Office of the Chief Executive Postdoctoral Fellowship scheme. KK and PS acknowledge Council of Scientific and Industrial Research- University Grants Commission, Government of India, for providing their research fellowships. The funders had no role in study design, data collection and analysis, decision to publish, or preparation of the manuscript.

**Competing Interests:** The authors have declared that no competing interests exist.

\* Email: gunjan.pandey@csiro.au

<sup>a</sup> Current address: Office of Chemical Safety, Department of Health, Phillip, ACT, Australia

<sup>b</sup> Current address: Environmental Earth System Science, Stanford University, Stanford, California, United States of America

<sup>c</sup> Current address: Hutchison/MRC Research Centre, University of Cambridge, Cambridge, United Kingdom

These authors contributed equally to this work.

## Introduction

Isomers of hexachlorocyclohexane (HCH) have been widely used as insecticides in various agricultural systems around the world for most of the last 70 years [1,2]. Despite mounting concerns about their human and eco-toxicity, they still find heavy use in some developing countries in particular [2,3]. Only the  $\gamma$  isomer is insecticidal but either a mixture of the four major isomers ( $\alpha$ ,  $\beta$ ,  $\gamma$  and  $\delta$ ), known as technical HCH, or purified  $\gamma$ -HCH, known as lindane, have been used commercially. The purification of lindane from technical HCH has led to massive dumps (> 50,000 tonnes) of the other isomers in several countries and the stability of all isomers (but particularly of  $\beta$ -HCH) has led to widespread contamination of the environment, originating both from the dump sites and broad scale agricultural uses [1–4].

Over 60 bacterial strains which can degrade HCH, about half of them Sphingomonads, have now been reported, and all those characterized biochemically and genetically have proven to use the well established Lin pathway (encoded by various *lin* genes) to degrade HCH [2,5,6]. There are two major forms of the pathway which differ in their initial reactions but subsequently converge. One form operates on  $\alpha$ -,  $\gamma$ - and  $\delta$ -HCH and is initiated by two

rounds of dehydrochlorination, followed by two rounds of hydrolytic dechlorination. The other form of the pathway operates on  $\beta$ - and  $\delta$ -HCH and is initiated by two rounds of hydrolytic dechlorination, albeit some of the subsequent steps remain to be elucidated. The *linA*/LinA gene/enzyme system catalyzes dehydrochlorinations in both forms of the pathway via an E2 reaction mechanism, and the *linB*/LinB gene/enzyme system catalyzes the hydrolytic dechlorinations via  $S_N2$  displacement reactions [2,5,6].

The LinB enzyme is a monomeric 32 kDa protein from the  $\alpha/\beta$  hydrolase fold superfamily [7]. Its structure has been solved [8] and its catalytic mechanism is reasonably well understood, with an Asp-His-Glu catalytic triad mediating nucleophilic attack on the substrate and then on an acyl-enzyme intermediate, and an oxyanion hole stabilizing the intermediate [9–12]. The best characterized LinB, LinB<sub>UT26A</sub> from *Sphingobium japonicum* strain UT26, has a broad substrate specificity, mainly due to a large active site volume, which includes monochloroalkanes (C3–C10), dichloroalkanes, bromoalkanes and chlorinated aliphatic alcohols [7,10]. Notably, this variant yields a significantly lower specificity constant for  $\beta$ -HCH ( $0.02 \text{ mM}^{-1} \text{ s}^{-1}$ ) as compared to another relatively well characterized LinB, namely, LinB<sub>B90A</sub>

(identical to LinB<sub>MI1205</sub>, and LinB<sub>BHC-A</sub> and LinB<sub>pLB1</sub>) from *Sphingobium indicum* strain B90A (0.20 mM<sup>-1</sup> s<sup>-1</sup>) [13]. Nonetheless the activity of LinB<sub>B90A</sub> for  $\beta$ -HCH is much lower than that of LinB<sub>UT26A</sub> for some of the other halogenated aliphatic compounds mentioned above (see [7,13] for a comprehensive list of kinetic constants).

A total of ten naturally occurring LinB variants have now been described which differ by as many as 16 (5.4%) of their amino acid residues [2]. At least some of these variants differ qualitatively in their substrate specificities; in addition to the  $\beta$ - and  $\delta$ -HCH difference above, LinB<sub>B90A</sub> will hydrolytically dechlorinate the metabolite tetrachlorocyclohexanol (TCDL), whereas LinB<sub>UT26</sub> does not [14]. A molecular dynamics simulation study suggests that this is mainly due to a difference in the flexibility of the entrance of the substrate access tunnel mediated by six out of the seven amino acid differences between the two enzyme variants [13].

Given the low but quantitatively different activities of the best characterized LinB<sub>UT26</sub> and LinB<sub>B90A</sub> variants for  $\beta$ - and  $\delta$ -HCH, and their quantitative differences in respect to TCDL, our aim in the work described herein has been to quantitatively assess the variation in the  $\beta$ - and  $\delta$ -HCH activities of all ten known naturally occurring LinB variants, plus another 13 synthetic variants derived on the basis of these data and the known structure of the LinB<sub>UT26</sub> protein. We find one synthetic variant with nearly 80-fold higher activity than LinB<sub>B90A</sub> for  $\beta$ -HCH and we suggest an explanation for its performance on the basis of increased mobility of its cap domain and increased affinity for the substrate.

## Materials and Methods

### Gene synthesis, expression vectors and chaperones

Codon optimized *linB* genes for expression in *E. coli* were synthesized by Genart AG, Regensburg Germany (Table S1). These genes were PCR amplified with respective attB1, attB2 and attB2-R2 primers (Table S2) and the amplicons were then cloned into pDONR201 and transferred to pDEST17, following the manufacturer's instructions (Invitrogen, CA). The host *E. coli* BL21-AI (Invitrogen) cells for some clones co-expressed chaperones from the plasmid pGro7 (Takara, Japan).

### Gene expression, enzyme purification and enzyme assays

Gene expression, enzyme purification and enzyme assays were performed as described earlier [15]. Briefly, the expression clones were grown in LB at 28°C until the OD<sub>600</sub> has reached 0.5. At this point L-(+) arabinose was added at a final concentration of 2 g/L. Cultures were grown overnight, cells were harvested by centrifugation and cell free extract was prepared in 10 mM imidazole buffer containing 1X Bugbuster solution (Novagen, Darmstadt). The cell free extract was centrifuged at 16,000 g for 20 min at 4°C and the supernatant was subject to the Ni<sup>2+</sup>-affinity chromatography to purify 6xHis-tagged enzyme using standard procedures. The purified enzymes were quantified using Nanodrop (Thermo Scientific, DE) and stored in storage buffer (pH 7.5) containing 10% glycerol and 1 mM 2-mercaptoethanol at 4°C. Enzyme assays were performed within 3 days of purification in a 500  $\mu$ l reaction mixture (final volume) containing 1.7  $\mu$ M of HCH in Tris glycine buffer (25 mM Tris, 193 mM Glycine, pH 8.3) at 22°C. The reaction was initiated by adding enzyme and terminated by adding 0.3% formic acid (final concentration). HCH depletion in the reaction was monitored by an electron capture detector coupled to a gas chromatograph as described earlier [15]. The enzyme assays were conducted in triplicate.

## Computational analysis

Atomistic models of LinB<sub>B90A</sub> as well as our most active mutant, LinB<sub>G2.2</sub>, were constructed by performing *in silico* mutagenesis on the LinB<sub>UT26</sub> structure (pdb 2BFN, [12]) with the Rosetta software suite. The appropriate residues were mutated and the surrounding non-catalytic residues were allowed to repack in accordance with the Rosetta fixed backbone protein design protocol [16]. During these calculations, the catalytic residues were kept in their crystallographic conformations while 500 cycles of repacking and optimization were performed and the lowest energy structure was retained. To construct models with  $\beta$ -HCH bound, the Rosetta enzyme design protocol was used to dock the transition state structure into the active site [17]. Restraints were added to keep  $\beta$ -HCH as close to the transition state as possible (the transition state was obtained from Brittain *et al.* based on their previous characterization of this reaction using electronic structure calculations [18]). Again, 500 cycles of repacking and optimization were performed and the lowest energy result was used. The reactant structure of  $\beta$ -HCH was fitted onto the transition state complex to yield a final conformation that was geometrically well posed for catalysis and still well described by a classical molecular mechanics energy function (Figure S1).

In order to assess the approximate affinity of LinB<sub>B90A</sub> and LinB<sub>G2.2</sub> for  $\beta$ -HCH, the Rosetta Ligand Dock program [19] was used to dock  $\beta$ -HCH into the apo structures of each enzyme. For each enzyme, 500 docking trajectories were computed. The results were first ranked by their total score (which approximates the overall stability of the model). The top 5% of these docked complexes were then ranked by their binding energy for  $\beta$ -HCH. The average binding energy was computed from the 10 best models.

Atomistic molecular dynamics simulations were performed on the apo and  $\beta$ -HCH-bound states of LinB<sub>B90A</sub> and LinB<sub>G2.2</sub>. These simulations were performed using the GROMACS 4.5.3 simulation package [20] (default parameters are used unless otherwise specified) with the AMBER99sb force field [21], the generalized Amber force field for  $\beta$ -HCH parameters [22], and the TIP3P explicit water model [23]. Temperature was kept at 298°K using the velocity-rescaling thermostat [24]. A 2-femtosecond timestep was used for all dynamics simulations with bond lengths constrained using the SHAKE algorithm [25]. Electrostatic interactions were calculated using the particle-mesh-Ewald method [26] with a cutoff of 15 Å. After minimization, simulations were equilibrated by running for 0.5 ns at constant volume and temperature with the positions of all non-solvent atoms harmonically restrained. Following this equilibration, the restraints were removed and a 30 ns production run was performed. Results were analysed using the VMD software package [27] and 3D structures were rendered using PyMOL (The PyMOL Molecular Graphics System, Version 1.3, Schrödinger, LLC).

## Results and Discussion

Eight of the ten natural LinB variants showed clearly measurable activities with both  $\beta$ - and  $\delta$ -HCH (Table 1). As expected from previous reports, LinB<sub>UT26</sub> yielded lower activities with either isomer [7,13,14], as did the closely related LinB<sub>SP4</sub>. The other eight variants all showed 10–20 fold greater activities with  $\beta$ - than  $\delta$ -HCH.

There was about a three-fold range of activities for each isomer across the latter eight variants. However, there was no obvious difference in activities across the three sequence-based groups of variants recognized by Lal *et al* [2] (again excluding LinB<sub>UT26</sub> and LinB<sub>SP4</sub>). Instead, there was considerable variation within their

**Table 1.** Activities towards β- and δ-HCH of the ten known naturally occurring LinB variants (organised according to the three sequence-based groups recognised by Lal et al [2], the thirteen synthetic mutants made herein, and the eight variants analysed by Ito et al [14].

LinB variants	Haplotypes																Turnover number (min <sup>-1</sup> )	
	2	6	7	81	83	112	134	135	138	147	150	222	223	224	247	253	β-HCH	δ-HCH
Group 3	W1.10			A			L	A	I						S		74±7	4±1
	W1.9			A		A	L	A	I						S		177±9	3±1
	W1.8				P	A	L	A	I						S	M	214±13	6±1
	W1.7					A	L	A	I						S	M	0*	0*
	W1.6			A		A	I	A	I						A	M	0*	0*
Group 2	W1.5	I	N	A	A					Y	M	V	H		A	M	124±13	6±1
Group 1	W1.4			A											S		170±15	8±1
	W1.3			A													154±31	8±1
	W1.2			A										V	S		65±9	5±0
	W1.1	S	K	P	T	A	V	T	L	D	L	A	I	A	H	I	90±1	4±1
Synthetic variants	G1.1				P												182±17	6±1
	G1.2						L										138±10	9±2
	G1.3							L									194±3	10±2
	G1.4								I								9±1	11±2
	G1.5														S		1±1	0*
	G1.6															M	20±1	0*
	G1.7			A	P										S		17±2	0*
	G1.8	I	N	A	A					Y	M	V	H		H	M	24±4	5±1
	G2.1			A	P												44±6	4±1
	G2.2						L	L									6920±272	241±6
	G2.3			A			L	L									422±12	31±6
	G2.4								I						S	M	10±2	3±1
	G2.5				P										S		4±1	2±1
Mutations from Ito et al. [13]				A		A	L	A	I						A	M	1.626	ND
	I134V			A		A	V	A	I						A	M	5.814	ND
	A247H			A		A	L	A	I						H	M	0.462	1.626
	I134V/A247H			A		A	V	A	I						H	M	1.458	ND
	LinB <sub>M120S/B90A</sub>																12.30	ND
	V134I						I										7.44	ND
	H247A														A		12.6	1.23
Activity (mM <sup>-1</sup> min <sup>-1</sup> )																		

Table 1. Cont.

LinB variants	Haplotypes																Turnover number (min <sup>-1</sup> )				
	2	6	7	81	83	112	134	135	138	147	150	222	223	224	247	253	β-HCH	δ-HCH			
V134I/H247A	.	.	.	.	.	.	I	.	.	.	.	.	.	.	A	.	6.24	ND			

V134I/H247A

6.24

ND

The LinB<sub>B90A</sub> is used as a reference sequence. All generation one (G1) and generation two (G2) mutants were derived from LinB<sub>B90A</sub>, except G1.7 and G1.8 which were derived from LinB<sub>SS04-3</sub> and LinB<sub>NM05</sub>, respectively. Activities determined herein are given as turnover numbers ( $\pm$  standard deviation) (min<sup>-1</sup>) and those from Ito et al [14] as specific activities (mM<sup>-1</sup> min<sup>-1</sup>). C indicates variants whose expression required the use of chaperones (see Material and Methods). ND = not determined. 0\* = <1 min<sup>-1</sup>.  
doi:10.1371/journal.pone.0103632.t001

two major groups (1 and 3 in Table 1), including some large differences between otherwise very closely related variants. The sequence differences between these variants frequently involved residues (eg 112, 134, 135, 138 and 253) constituting the enzyme's active site.

Based on the above results, six generation one synthetic variants (denoted G1.1–G1.6) on the LinB<sub>B90A</sub> background and one synthetic variant each on the LinB<sub>SS04-3</sub> (G1.7) and LinB<sub>NM05</sub> (G1.8) background were made. One of the former (G1.3; T135L) was generated by mistake (physio-chemically similar T135A was intended) during gene synthesis. These eight generation one mutants were analyzed for β- and δ-HCH activities in order to determine the contributions of individual amino acid differences to the activity variation. Three LinB<sub>B90A</sub> variants (G1.1–G1.3) showed ~2 fold higher activity (Table 1), and these mutations (A83P, V134L and T135L), along with certain others, were used to make five second generation double and triple mutants on the LinB<sub>B90A</sub> background. These mutants were also tested on β- and δ-HCH.

Overall eleven of the synthetic variants from both generations one and two yielded activity values within the range seen for the natural variants (0–214 and 0–8 min<sup>-1</sup> for β- and δ-HCH respectively; Table 1). However, LinB<sub>G2.3</sub> and LinB<sub>G2.2</sub> yielded activities 2–4 and 30 fold, respectively, higher than any previously seen, and 4–8 and about 80 fold higher than those of the LinB<sub>B90A</sub> reference variant (Table 1). β-HCH activities were again much higher than δ-HCH for all the synthetic variants and there was a strong correlation between β- and δ-HCH activities across the total of 23 natural and synthetic variants ( $r^2 = 0.99$ ;  $P < 0.03$ ).

Table 2 rearranges a subset of the data from Table 1 to show the effects of single amino acid differences at eight positions spread across the enzyme (T81A, A83P, V112A, V134L, T135L, L138I, H247S and I253M). In six of these cases the effects of each substitution could be examined in more than one haplotype background. All eight substitutions had significant effects in at least one, and generally, most of the backgrounds tested. For six of the substitutions the effect was 10 fold or greater. Notably however, all six substitutions tested in more than one background also showed significant, and often also large, effects of the background haplotype. The table shows clear cases of positive (V134L/T135L in LinB<sub>G2.2</sub>) and negative epistasis (A81 and P83 producing two-fold increases in β- and δ-HCH activities alone but a two-fold decrease together). Also a comparison of the A83P mutation in LinB<sub>B90A</sub> and LinB<sub>SS04-3</sub> illustrates the effect of the genetic background; this mutation doubled activity in the LinB<sub>B90A</sub> background but decreased it by 10 fold in the LinB<sub>SS04-3</sub> background.

The fact that the use of chaperones was necessary for expression of a few variants with higher activity suggests that some of the mutations nevertheless were deleterious for protein solubility or stability. We are now exploring whether the chaperone dependency of these variants could be ameliorated by stabilizing mutations.

Molecular dynamics simulations were used to probe the conformational dynamics of the synthetic LinB<sub>G2.2</sub> variant relative to LinB<sub>B90A</sub> (our reference variant). These simulations revealed large differences in conformational flexibility within the cap domain (Figure 1). This domain occludes the active site and has previously been shown to be more flexible in LinB relative to the related dehalogenases DhaA and DhlA [28]. Here we see that LinB<sub>G2.2</sub> shows greatly enhanced flexibility in this region when compared to LinB<sub>B90A</sub>. Unlike some of the other variants of this enzyme, LinB<sub>B90A</sub> has a histidine at position 247. This residue has been hypothesized to enhance activity by reducing solvent access

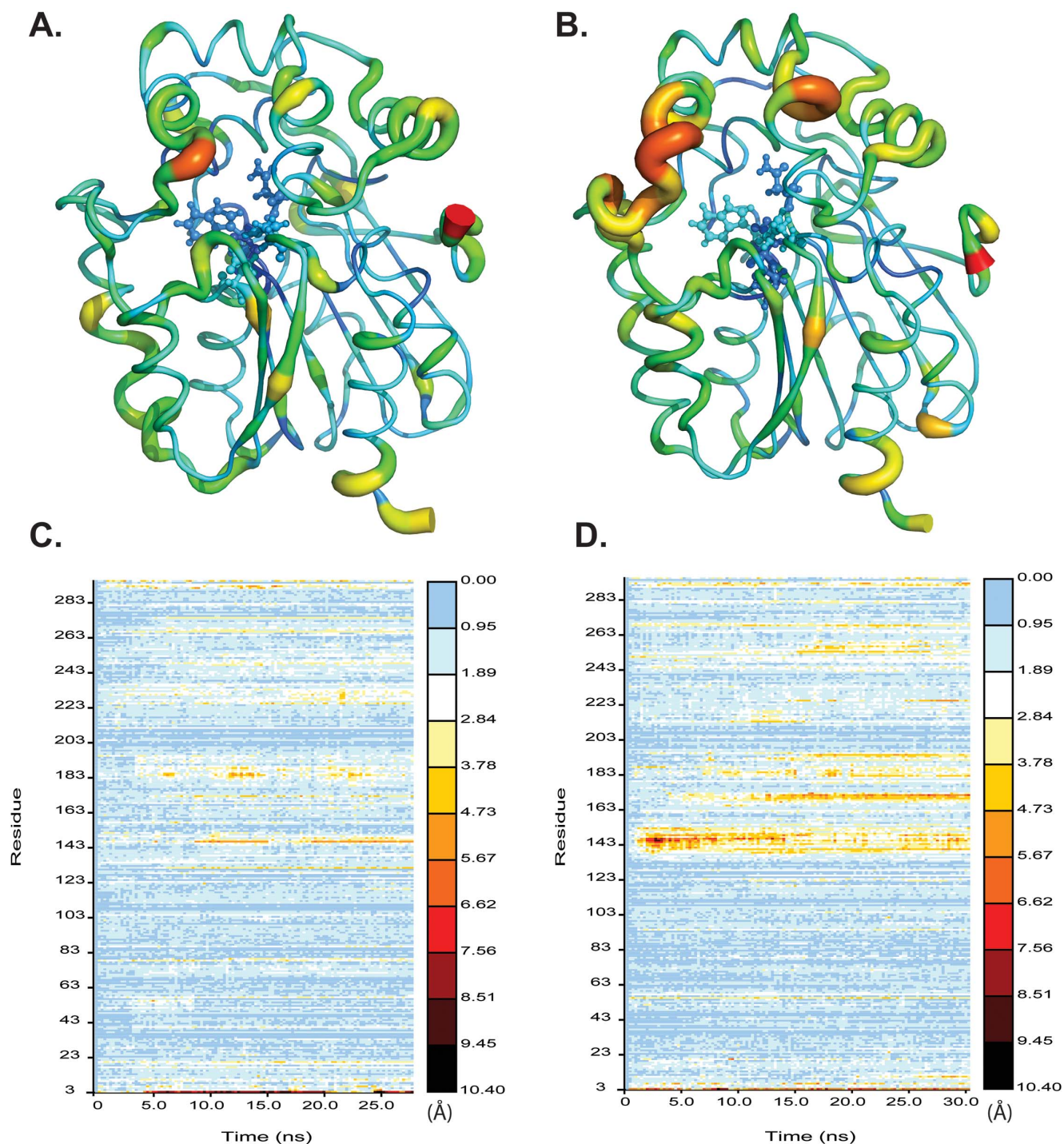
**Table 2.** Pairwise comparisons of  $\beta$ - and  $\delta$ -HCH data for variants characterized herein which differ by single amino acid changes.

Residues	Mutants	Haplotype																Turnover number ( $\text{min}^{-1}$ )	
		2	6	7	81	83	112	134	135	138	147	150	222	223	224	247	253	$\beta$ -HCH	$\delta$ -HCH
		S	K	P	T	A	V	V	T	L	D	L	A	I	A	H	I		
T81A	W1.1/W1.3	.	.	.	T/A	.	.	.	.	.	.	.	.	.	.	.	.	90 $\pm$ 1/154 $\pm$ 31	4 $\pm$ 1/5 $\pm$ 1
T81A	G2.2/G2.3	.	.	.	T/A	.	.	L	L	.	.	.	.	.	.	.	.	6920 $\pm$ 272/422 $\pm$ 12	241 $\pm$ 6/31 $\pm$ 6
T81A	G2.5/G2.1	.	.	.	T/A	P	.	.	.	.	.	.	.	.	.	.	.	4 $\pm$ 1/44 $\pm$ 6	2 $\pm$ 1/4 $\pm$ 1
A83P	W1.1/G1.1	.	.	.	.	A/P	.	.	.	.	.	.	.	.	.	.	.	90 $\pm$ 1/182 $\pm$ 17	4 $\pm$ 1/6 $\pm$ 1
A83P	W1.3/G2.1	.	.	.	A	A/P	.	.	.	.	.	.	.	.	.	.	.	154 $\pm$ 31/44 $\pm$ 6	5 $\pm$ 1/4 $\pm$ 1
A83P	W1.7/W1.8	.	.	.	.	A/P	A	L	A	I	.	.	.	.	.	S	M	0/214 $\pm$ 13	0/6 $\pm$ 1
A83P	W1.4/G1.7	.	.	.	A	A/P	.	.	.	.	.	.	.	.	.	S	.	170 $\pm$ 15/17 $\pm$ 2	8 $\pm$ 1/0
V112A	W1.10/W1.9	.	.	.	A	.	V/A	L	A	I	.	.	.	.	.	S	.	74 $\pm$ 7/177 $\pm$ 9	4 $\pm$ 1/3 $\pm$ 1
V134L	W1.1/G1.2	.	.	.	.	.	.	V/L	.	.	.	.	.	.	.	.	.	90 $\pm$ 1/138 $\pm$ 10	4 $\pm$ 1/9 $\pm$ 2
V134L	G1.3/G2.2	.	.	.	.	.	.	V/L	L	.	.	.	.	.	.	.	.	194 $\pm$ 3/6920 $\pm$ 272	10 $\pm$ 2/241 $\pm$ 6
T135L	W1.1/G1.3	.	.	.	.	.	.	.	T/L	.	.	.	.	.	.	.	.	90 $\pm$ 1/194 $\pm$ 3	4 $\pm$ 1/10 $\pm$ 2
T135L	G1.2/G2.2	.	.	.	.	.	.	L	T/L	.	.	.	.	.	.	.	.	138 $\pm$ 10/6920 $\pm$ 272	9 $\pm$ 2/241 $\pm$ 6
L138I	W1.1/G1.4	.	.	.	.	.	.	.	.	L/I	.	.	.	.	.	.	.	90 $\pm$ 1/9 $\pm$ 1	4 $\pm$ 1/11 $\pm$ 2
H247S	W1.1/G1.5	.	.	.	.	.	.	.	.	.	.	.	.	.	.	H/S	.	90 $\pm$ 1/1 $\pm$ 1	4 $\pm$ 1/0
H247S	W1.3/W1.4	.	.	.	A	.	.	.	.	.	.	.	.	.	.	H/S	.	154 $\pm$ 31/170 $\pm$ 15	5 $\pm$ 1/8 $\pm$ 1
H247S	G2.1/G1.7	.	.	.	A	P	.	.	.	.	.	.	.	.	.	H/S	.	44 $\pm$ 6/17 $\pm$ 2	4 $\pm$ 1/0
I253M	W1.1/G1.6	.	.	.	.	.	.	.	.	.	.	.	.	.	.	.	I/M	90 $\pm$ 1/20 $\pm$ 1	4 $\pm$ 1/0

The activity data are taken from Table 1 and abbreviated variant names are also as in Table 1. Haplotypes are also shown as per Table 1 (with LinB<sub>990A</sub> again used as the reference), except that residues that did not differ among the subset of variants included in these comparisons have been omitted. Blue and red colours are used to show the residues and activities corresponding to each variant in the pairwise comparisons.

doi:10.1371/journal.pone.0103632.t002



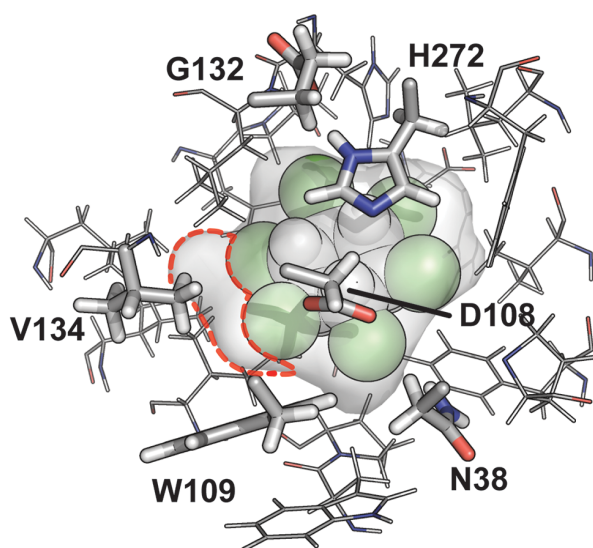
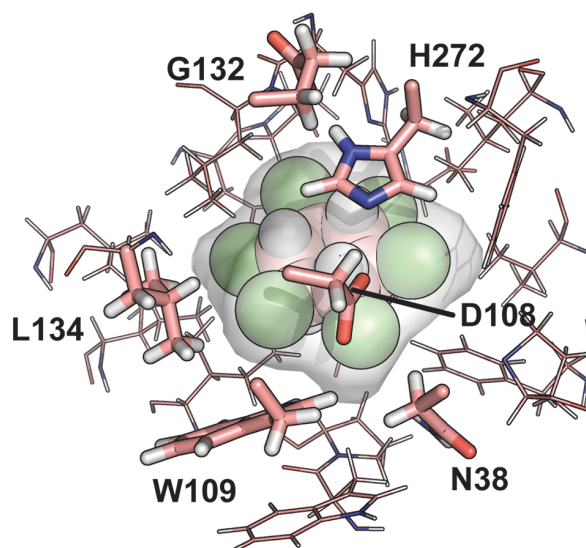


**Figure 1. Comparative conformational flexibility within the cap domain of two LinB variants.** Sausage diagram for LinB<sub>B90A</sub> (A) and LinB<sub>G2.2</sub> (B) in which the thickness of the chain as well as the colour denotes the average RMSD of each residue. The active site catalytic residues are rendered in ball and stick. The RMSD of each residue as a function of time is plotted for LinB<sub>B90A</sub> (C) and LinB<sub>G2.2</sub> (D).  
doi:10.1371/journal.pone.0103632.g001

to the active site [13]. Although this mechanism may be feasible for some of the smaller haloalkane dehalogenase substrates (such as dichloroethane and trichloropropane), HCH cannot easily diffuse into the partially occluded active site in LinB, nor can it easily enter through the side tunnels previously characterized for this enzyme [13]. As such, it seems reasonable to assume that increased flexibility in the cap domain plays an important role in

the enhancement of catalysis as observed in LinB<sub>G2.2</sub> relative to LinB<sub>B90A</sub> by removing kinetic barriers to substrate binding (in spite of the fact that this potentially allows greater solvent penetration into the active site).

Additionally, our simulations indicate that LinB<sub>G2.2</sub> is able to bind  $\beta$ -HCH more tightly than LinB<sub>B90A</sub>. The average binding energy of  $\beta$ -HCH to LinB<sub>G2.2</sub> was calculated to be  $-4.25 \pm 0.13$

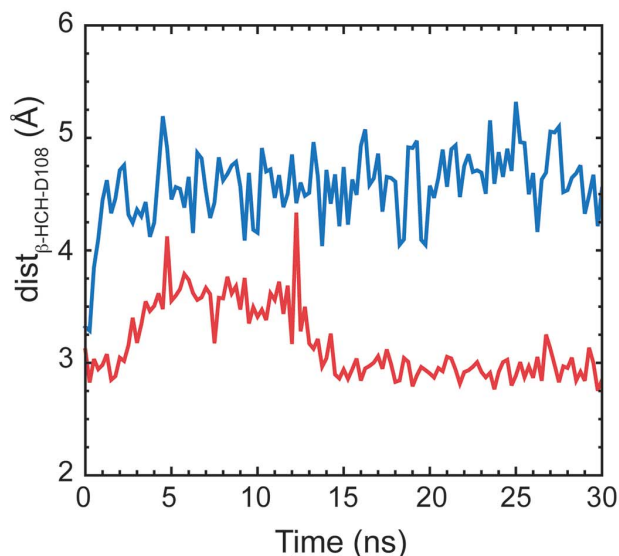
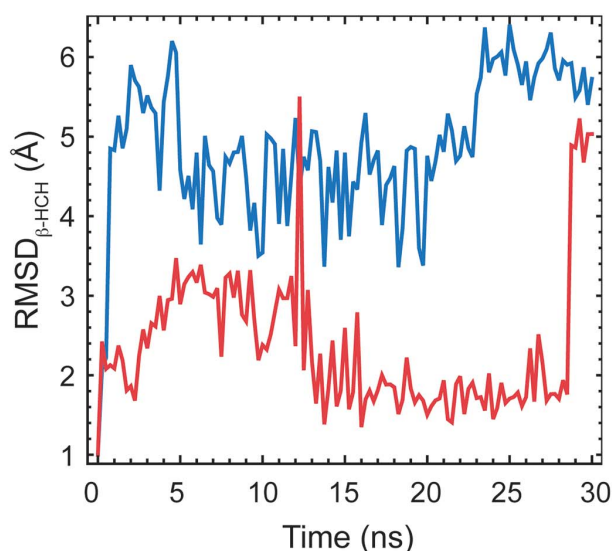
**A.****B.**

**Figure 2. Approximate affinity of LinB<sub>B90A</sub> and LinB<sub>G2.2</sub> for  $\beta$ -HCH using Rosetta Ligand Dock program.** Highest scoring docked pose for LinB<sub>B90A</sub> (A) and LinB<sub>G2.2</sub> (B). The ligand  $\beta$ -HCH is shown as Van der Waals spheres, catalytic residues (as well as residue 134 which differs between LinB<sub>B90A</sub> and LinB<sub>G2.2</sub>) are rendered as thick sticks. Other residues within 5 Å of  $\beta$ -HCH are rendered as thin sticks. The empty space in the binding pocket of LinB<sub>B90A</sub> that is filled by the V134L mutation of LinB<sub>G2.2</sub> is outlined with red dashes.  
doi:10.1371/journal.pone.0103632.g002

REU (Rosetta energy units) compared to that of LinB<sub>B90A</sub>, which was  $-2.54 \pm 0.22$ . This modest increase in affinity arises in part from more favourable hydrophobic interactions between L134 and  $\beta$ -HCH (Figure 2). This is also supported by results from molecular dynamics simulations with  $\beta$ -HCH bound, which show that LinB<sub>G2.2</sub> is able to keep the ligand much closer to the catalytic conformation than LinB<sub>B90A</sub> (Figure 3). Both the distance between

the nucleophilic oxygen and the ligand centre of mass as well as the RMSD from the catalytic conformation are much lower for LinB<sub>G2.2</sub> relative to LinB<sub>B90A</sub> (Figure 3).

Collectively, these results imply that the V134L/T135L mutations of LinB<sub>G2.2</sub> enhance catalysis by affecting the conformational plasticity of the cap domain and by holding the substrate in a suitable conformation for catalysis. More extensive simula-

**A.****B.**

**Figure 3. Molecular dynamics simulations of LinB with  $\beta$ -HCH bound in the active site.** The distance between the nucleophilic oxygen of Asp108 and the center of mass of  $\beta$ -HCH is shown as a function of time (LinB<sub>B90A</sub> in blue and LinB<sub>G2.2</sub> in red) in panel A. Panel B shows the RMSD from the near-attack conformation for  $\beta$ -HCH as a function of time (LinB<sub>B90A</sub> in blue and LinB<sub>G2.2</sub> in red) in panel B.  
doi:10.1371/journal.pone.0103632.g003

tions as well as additional biophysical and biochemical analysis are now needed to provide a more complete picture of the relevant conformational motions of this enzyme.

## Supporting Information

**Figure S1 Superposition of the ground state  $\beta$ -HCH structure and the  $\beta$ -HCH transition state as calculated by *ab initio* electronic structure theory.**

(DOCX)

**Table S1 Enzyme variants and primers.**

(DOCX)

**Table S2 Codon optimized gene sequences.**

(DOCX)

## References

- Vijgen J, Abhilash PC, Li YF, Lal R, Forter M, et al. (2011) Hexachlorocyclohexane (HCH) as new Stockholm Convention POPs - a global perspective on the management of lindane and its waste isomers. *Environ Sci Pollut Res Int* 18: 152–162.
- Lal R, Pandey G, Sharma P, Kumari K, Malhotra S, et al. (2010) Biochemistry of microbial degradation of hexachlorocyclohexane and prospects for bioremediation. *Microbiol Mol Biol Rev* 74: 58–80.
- Jit S, Dadhwal M, Kumari H, Jindal S, Kaur J, et al. (2011) Evaluation of hexachlorocyclohexane contamination from the last lindane production plant operating in India. *Environ Sci Pollut Res Int* 18: 586–597.
- Weber R, Gaus C, Tysklind M, Johnston P, Forter M, et al. (2008) Dioxin- and POP-contaminated sites-contemporary and future relevance and challenges. *Environ Sci Pollut Res Int* 15: 363–393.
- Lal R, Dogra C, Malhotra S, Sharma P, Pal R (2006) Diversity, distribution and divergence of *lin* genes in hexachlorocyclohexane-degrading sphingomonads. *Trends Biotechnol* 24: 121–130.
- Nagata Y, Endo R, Ito M, Ohtsubo Y, Tsuda M (2007) Aerobic degradation of lindane (gamma-hexachlorocyclohexane) in bacteria and its biochemical and molecular basis. *Appl Microbiol Biotechnol* 76: 741–752.
- Nagata Y, Miyauchi K, Damborsky J, Manova K, Ansorgova A, et al. (1997) Purification and characterization of a haloalkane dehalogenase of a new substrate class from a gamma-hexachlorocyclohexane-degrading bacterium, *Sphingomonas paucimobilis* UT26. *Appl Environ Microbiol* 63: 3707–3710.
- Marek J, Vevodova J, Smananova IK, Nagata Y, Svensson LA, et al. (2000) Crystal structure of the haloalkane dehalogenase from *Sphingomonas paucimobilis* UT26. *Biochemistry* 39: 14082–14086.
- Bohac M, Nagata Y, Prokop Z, Prokop M, Monincova M, et al. (2002) Halide-stabilizing residues of haloalkane dehalogenases studied by quantum mechanic calculations and site-directed mutagenesis. *Biochemistry* 41: 14272–14280.
- Damborsky J, Koca J (1999) Analysis of the reaction mechanism and substrate specificity of haloalkane dehalogenases by sequential and structural comparisons. *Protein Eng* 12: 989–998.
- Hynkova K, Nagata Y, Takagi M, Damborsky J (1999) Identification of the catalytic triad in the haloalkane dehalogenase from *Sphingomonas paucimobilis* UT26. *FEBS Lett* 446: 177–181.
- Oakley AJ, Klvana M, Otyepka M, Nagata Y, Wilce MCJ, et al. (2004) Crystal structure of haloalkane dehalogenase LinB from *Sphingomonas paucimobilis* UT26 at 0.95 angstrom resolution: dynamics of catalytic residues. *Biochemistry* 43: 870–878.
- Okai M, Ohtsuka J, Imai LF, Mase T, Moriuchi R, et al. (2013) Crystal structure and site-directed mutagenesis analyses of haloalkane dehalogenase LinB from *Sphingobium* sp. strain MI1205. *J Bacteriol* 195: 2642–2651.
- Ito M, Prokop Z, Klvana M, Otsubo Y, Tsuda M, et al. (2007) Degradation of beta-hexachlorocyclohexane by haloalkane dehalogenase LinB from gamma-hexachlorocyclohexane-utilizing bacterium *Sphingobium* sp. MI1205. *Arch Microbiol* 188: 313–325.
- Sharma P, Pandey R, Kumari K, Pandey G, Jackson CJ, et al. (2011) Kinetic and sequence-structure-function analysis of known LinA variants with different hexachlorocyclohexane isomers. *PLoS One* 6: e25128.
- Kuhlman B, Dantas G, Ireton GC, Varani G, Stoddard BL, et al. (2003) Design of a novel globular protein fold with atomic-level accuracy. *Science* 302: 1364–1368.
- Richter F, Leaver-Fay A, Khare SD, Bjelic S, Baker D (2011) De novo enzyme design using Rosetta3. *PLoS ONE* 6: e19230.
- Brittain DRB, Pandey R, Kumari K, Sharma P, Pandey G, et al. (2011) Competing S(N)<sub>2</sub> and E2 reaction pathways for hexachlorocyclohexane degradation in the gas phase, solution and enzymes. *Chem Commun* 47: 976–978.
- Lemmon G, Meiler J (2012) Rosetta Ligand docking with flexible XML protocols. *Methods Mol Biol* 819: 143–155.
- Pronk S, Pall S, Schulz R, Larsson P, Bjelkmar P, et al. (2013) GROMACS 4.5: A high-throughput and highly parallel open source molecular simulation toolkit. *Bioinformatics* 29: 845–854.
- Hornak V, Abel R, Okur A, Strockbine B, Roitberg A, et al. (2006) Comparison of multiple Amber force fields and development of improved protein backbone parameters. *Proteins* 65: 712–725.
- Wang J, Wolf RM, Caldwell JW, Kollman PA, Case DA (2004) Development and testing of a general amber force field. *J Comput Chem* 25: 1157–1174.
- Jorgenson WL, Chandrasekhar J, Madura JD (1983) Comparison of simple potential functions for simulating liquid water. *J Chem Phys* 79: 926–935.
- Bussi G, Donadio D, Parrinello M (2007) Canonical sampling through velocity rescaling. *J Chem Phys* 126: 14101–14107.
- Ryckaert J-P, Ciccotti G, Berendsen HJC (1977) Numerical integration of the cartesian equations of motion of a system with constraints: molecular dynamics of n-alkanes. *J Comput Phys* 23: 327–341.
- Darden T, York D, Pedersen L (1993) Particle mesh Ewald: An N log(N) method for Ewald sums in large systems. *J Chem Phys* 98: 10089–10092.
- Humphrey W, Dalke A, Schulten K (1996) VMD: visual molecular dynamics. *J Mol Graph* 14: 33–38.
- Pavlova M, Klvana M, Prokop Z, Chaloupkova R, Banas P, et al. (2009) Redesigning dehalogenase access tunnels as a strategy for degrading an anthropogenic substrate. *Nat Chem Biol* 5: 727–733.

## Acknowledgments

We thank Nikki Dellas and Stephen Pearce for critically reading the manuscript.

## Author Contributions

Conceived and designed the experiments: RP DL RL JGO GP. Performed the experiments: RP DL KK PS. Analyzed the data: RP DL KK PS JGO GP. Contributed reagents/materials/analysis tools: DL JGO GP. Contributed to the writing of the manuscript: RP DL JGO GP.